학술상강연

알루미늄 합금의 표면경화

이 영 호
(충남대학교 공대 기계공학과 교수)

Table 1 Chemical composition of base metal.

Material	Chemical compositions (wt.%)						
	Si	Fe	Cu	Mn	Mg	Zn	Al
AC2B	5.8	0.49	2.5	0.31	0.04	0.08	Bal.

* Size of test specimen 100'x 60"x 10'

Powder	Size(μm)	Morphology of powder (SEM)
Cr	50~100	
Cu	43~50	
Ni	65~150	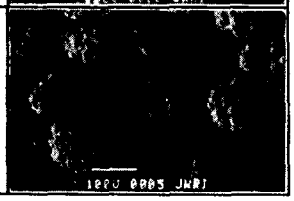

Fig. 1 Grain size and shape of metal powder.

length ×60 mm in width ×10 mm in thickness.

As a metal powder for alloying, chromium (Cr), copper (Cu) and nickel (Ni) powders of 99.9% in purity were used. The shape and grain size of these powders are shown in **Fig. 1**. Cr is the crushed and Cu and Ni are the atomized powders.

According to phase diagrams[13], in Al rich side in each binary system, these elements show peritectic reaction in Al-Cr, single eutectic reaction in Al-Cu and eutectic-peritectic reactions in Al-Ni systems, which is an intermediate one between Al-Cr and Al-Cu systems.

Prior to overlaying, these powders were dried in vacuum (1×10^{-1}Pa, 20°C, 24h) to intend to eliminate the formation of porosity in alloyed bead, but this pretreatment showed almost no effect for preventing porosity in this study.

2.2 Experimental procedures

2.2.1 PTA overlaying process

Figure 2 shows the schematic illustration explaining the

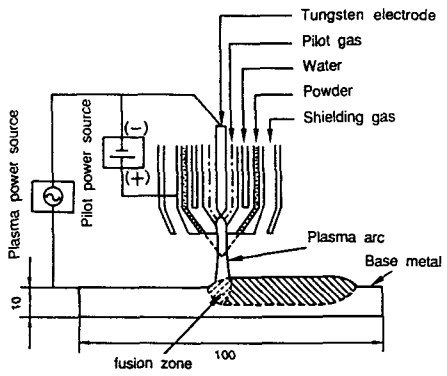

Fig. 2 Schematic illustration of PTA overlaying process.

principle of PTA overlaying process. Surface layer of base metal is melted continuously by plasma arc with a constant traveling speed, and simultaniously metal powder is fed into the molten pool through plasma torch and plasma arc and then react with molten Al to make alloyed layer on Al base metal surface.

An inverter type alternate current plasma transferred arc overlaying equipment with a powder feeder was used. Overlaying conditions used are shown in **Table 2**. The alternate frequency is 200Hz, time duration ratio of electrode negative (T_{EN}) and electrode positive (T_{EP}) is $T_{EN}/T_{MEAN}=75/25$, and mean current (I_{MEAN}, which is called overlaying current in this study) ranged from 125A to 200A by changing the negative current (I_{EN}) under the constant positive current (I_{EP}) of 80A. Overlaying speed was 150 mm/min and the distance between a tip of torch and base metal surface was 8 mm, which corresponded to the crosspoint of powder streams from different injection holes in a torch tip. Argon gas was employed as a shielding gas. Powder feeding rate was varied from 5 to 20 g/min for each powder at a constant carrier Ar gas of 2 l/min.

2.2.2 Structural observation of alloyed bead

A crosssection of alloyed bead (which means overlayed bead) was electrolitically polished in 2.5%HBF_4 water

Table 2 Overlaying conditions used.

I MEAN (A)	I EN (A)	I EP (A)	TEN / TEP	Powder feeding rate (g/min)	Overlaying speed (mm/min)	Ar gas (l/min)		
						Pilot gas	Powder carrier gas	Shield. gas
125	172	80	75/25	5 ~ 20	150	0.5	2	16
150	217							
175	255							
200	295							

solution (15V, 10sec), and after then optical and scanning electron microscopic observations, alloyed element distribution measurement by EPMA and phase idintification by EPMA and X-ray diffractometry were performed.

2.2.3 Hardness and wear resistance measurements

Hardness of alloyed bead was measured with vickers microhardness tester with 9.8N load on crosssection.

Wear resistance of alloyed bead was measured with Ogoshi-type wear tester. A rorating counter disk of SUJ2(Hv650), 30 mm in diameter, was pressed on a polished alloyed bead surface under the constant test condition of 9.8N in wear load, 4.36 m/sec in rotating speed and 100 m in wear distance and then wear volume of alloyed bead was measured.

2.2.4 Residual gas analysis in blow hole

Alloyed bead was drilled from the surface in order to cut blow hole in a vacuum chamber (1×10^{-5}Pa) and simultaniously the kind of gas exhausted from blow hole was measured with 4 polers mass spectroscopy.

3. Experimental Results and Discussions

3.1 Alloyed bead appearance

Figure 3 shows the typical appearance of Cu alloyed bead for different overlaying current and powder feeding rate. At low current as 125A, as the surface melting of base metal was not sufficient, excess powders fed were scattered and/or deposited on its surface as a spherical droplet. At high feeding rate as 20 g/min, excess powders were hilled up on its surface. Almost the same phenomena were observed in Cr and Ni alloyed beads.

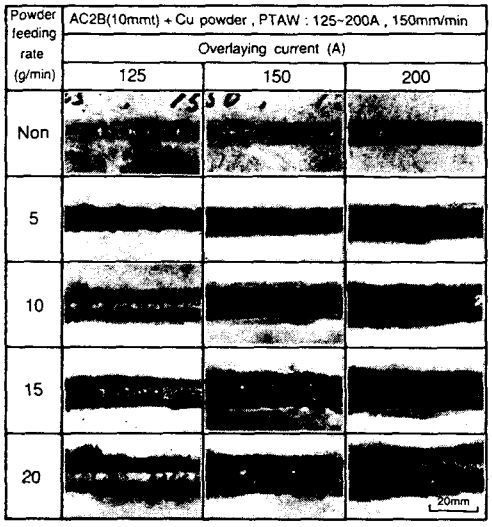

Fig. 3 General appearance of Cu alloyed bead surface

Figure 4 shows schematically the combined effect of overlaying current and powder feeding rate for Cr, Cu and Ni powders on the bead appearance, of which surface condition was divided into 3 types designated by marks in figures.

The optimum condition range with a smooth surface was obtained with more than 150A, and the optimum range of

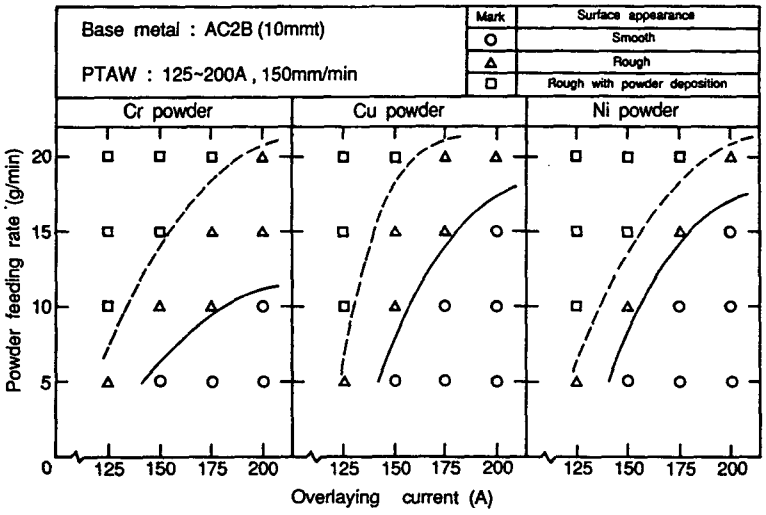

Fig. 4 Combined effect of overlaying current and powder feeding rate on alloyed bead appearance.

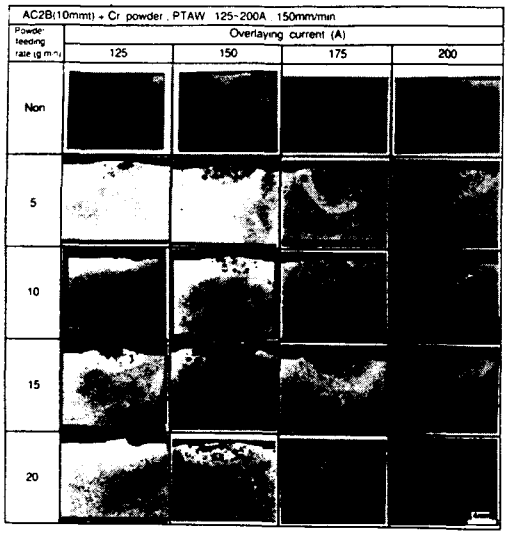

(a) Cr alloyed bead

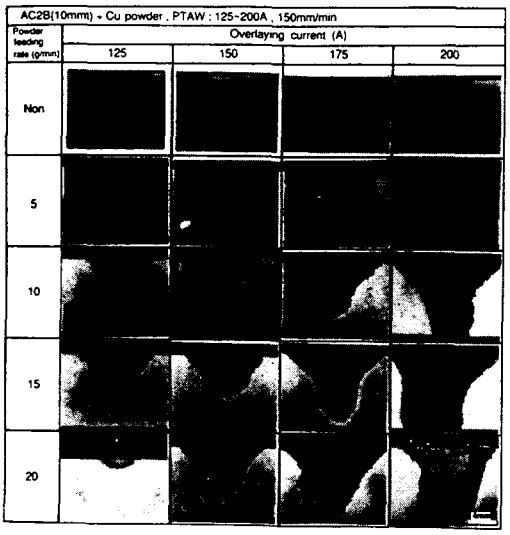

(b) Cu alloyed bead

Fig. 5 Combined effect of overlaying current and powder feeding rate on macrostructure of crosssection of alloyed bead.

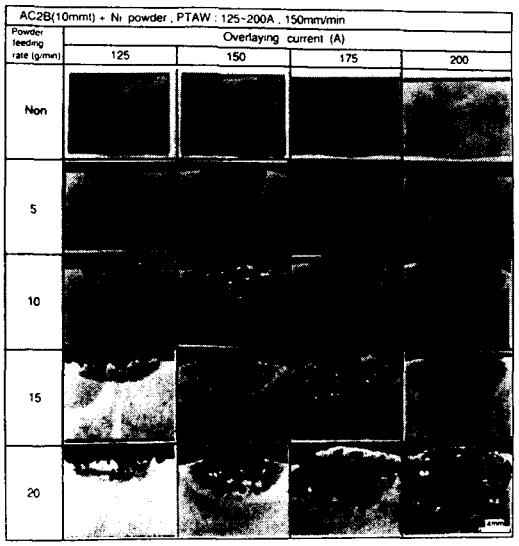

(c) Ni alloyed bead

powder feeding rate was enlarged by the increase of overlaying current. Such optimum condition range was much wider in the case of Cu and Ni powders than Cr powder. This result means that Cu and Ni are better alloying powders in a viewpoint of the easiness of alloyed bead formation. The reasons are considered to be related to Al binary phase diagram. Details will be discussed in the latter section.

3.2 Crosssectional shape of alloyed bead

Figure 5 (a), (b) and **(c)** shows the combined effect of powder feeding rate and overlaying current on the macrostructures of crosssections of alloyed bead for Cr, Cu and Ni powders, respectively. Bead width and penetration depth were increased by the powder feeding rate for each alloying powder from those without powder, though much differences were observed by the kind of powder.

In case of Cr (a), bead width and penetration depth were much smaller than those of Cu and Ni alloyed beads. Penetration depth was increased at first as the powder feeding rate, but subsequently it was decreased. It is considered that the increase in penetration depth is due to the heat of formation of intermetallic compound in bead (13 kJ/ mol in case of $CrAl_7$)[14]. However, As much increase in feeding rate, bead surface became covered with high temperature compound layer, because Cr was easy to make high temperature compound with molten Al by peritectic reaction, and this caused the decrease in penetration depth and ununiform distribution of structure.

In case of Cu (b), on the contraty, bead width and penetration depth were monotonously increased as the

increase of feeding rate, and even with lower current than 150A deep penetration and uniform structure were obtained. The reason why Cu can make good alloyed bead so easily on Al alloy surface under the wide overlaying condition range is considered as follows: Cu has a eutectic reaction with Al at low temperature (eutectic temperature 548°C) in a wide composition range as shown in Al-Cu phase diagram (Fig. 11 (a)). In addition to this, liquidus temperature remains comparably low as high as 591°C even with hyper-eutectic composition. These features can lead the easy and uniform melting and the alloying between Al base metal and Cu powder fed.

In case of Ni (c), when Ni powder feeding rate was low, bead width and penetration depth were increased remarkably as same as Cu or more and macrostructure was almost uniform. However, as the feeding rate exceed the critical value, penetration depth was decreased and the structure became ununiform. According to Al-Ni phase diagram (Fig. 14 (a)), there is an eutectic reaction at comparably low eutectic temperature (640°C) in a low Ni content. In addition, comparably large formation heats of $NiAl_3$ and Ni_2Al_3, that is, 40 and 57 kJ/mol[14], respectively contributed to the increase of penetration depth and the easy formation of uniform alloyed bead within lower feeding rate.

However, as the increase of Ni content, peritectic reactions began to be appeared, and liquidus temperature steeply raised to make it easy to form high temperature intermetallic compound. Therefore, in case of higher feeding rate, penetration depth was decreased because the high temperature compound layer covered the bead surface as same as Cr.

The condition range for uniform structure in alloyed bead in Fig. 5 coincided with that for the optimum range for the smooth bead surface in Fig. 4 in the case of Cr and Ni and was much wider than the optimum condition range in the case of Cu.

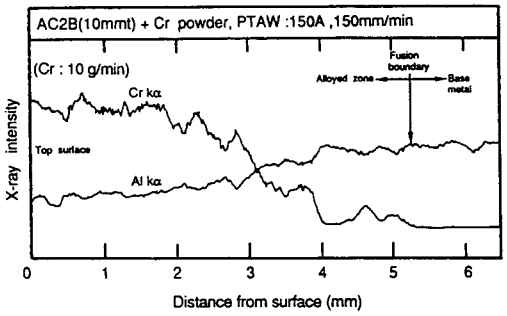

Fig. 7 Distribution of Cr and Al in Cr alloyed bead at powder feeding rate, 10 g/min.

Consequently, Cu has the widest condition range to obtain the uniform alloyed bead and Ni followed, and Cr has the narrowest range.

3.3 Microstructure of alloyed bead

3.3.1 Cr alloyed bead

Figure 6 shows the typical microstructural changes of the top, middle and bottom zones of alloyed bead with different powder feeding rate. Some black holes in figures seem to be blow holes.

It is difficult to get a uniform structure in Cr alloyed bead and the amount of compound was increased gradually from the bottom to top zones of the bead. The alloyed bead consisted of a needle structure at powder feeding rate of 5 g/min, needle and globular structures at 10 g/min, and globular and layer structures in the top zone and needle and globular structures in the middle and bottom zones at more than 15 g/min. Cracking was observed in such compound layer because of the luck of ductility of brittle

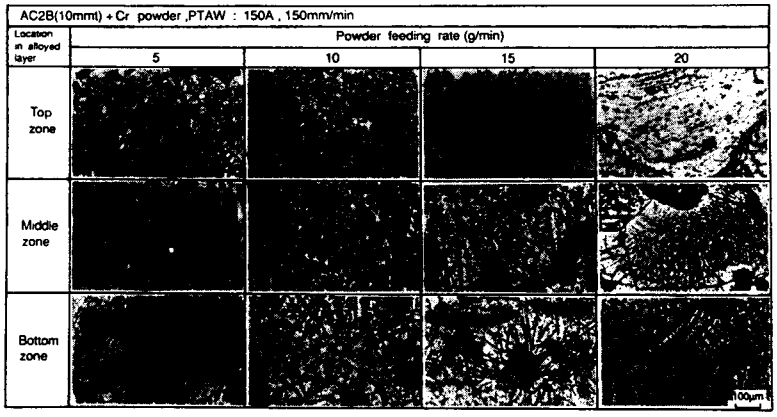

Fig. 6 Microstructures of Cr alloyed bead at different powder feeding rate.

compounds and tensile residual stress built up in the cooling stage after overlaying process.

Figure 7 shows Cr and Al distributions from the top to bottom zones in crosssections of the beads with 10 g/min. Cr distribution in the bead was also ununiform, that is, high Cr content in the top zone and abrupt decrease in the bottom zone were observed, which corresponding to the unumiform structure as shown in Fig. 6.

Figure 8 shows the relation between Al-Cr phase diagram (a) and SEM microstructures with mean Cr contents of (b) 8.0, (c) 17.0 and (d) 26.9wt% corresponding to the bottom, middle and top zones, respectively. Microstructures with 8 and 17wt%Cr consisted of primary compounds of Cr_2Al_{11}(b) and $CrAl_4$(c) surrounding with α(Al)+$AlCr_7$ eutectic (a), respectively. With increased Cr content of 26.9wt%, it became dense and consisted of mainly Cr_2Al_{11} and Cr_4Al_9(d) and partly α(Al)+$AlCr_7$ eutectic. At more than 15 g/min, surface compound layer consisted mainly of Cr_5

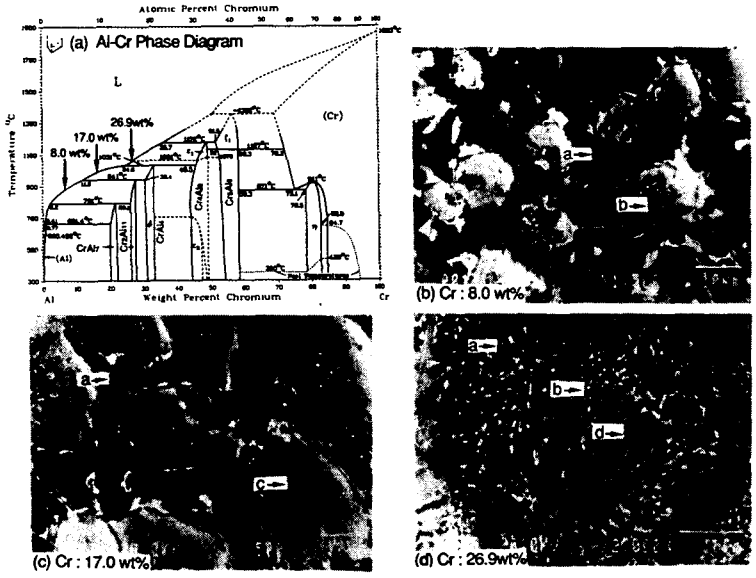

Fig. 8 SEM microstructures and mean Cr content at bottom (b), middle (c) and top zones (d) of Cr alloyed bead showing relationship between phase diagram and phase formed, a: α(Al)+$CrAl_7$, b: Cr_2Al_{11}, c: $CrAl_4$, d: Cr_4Al_9.

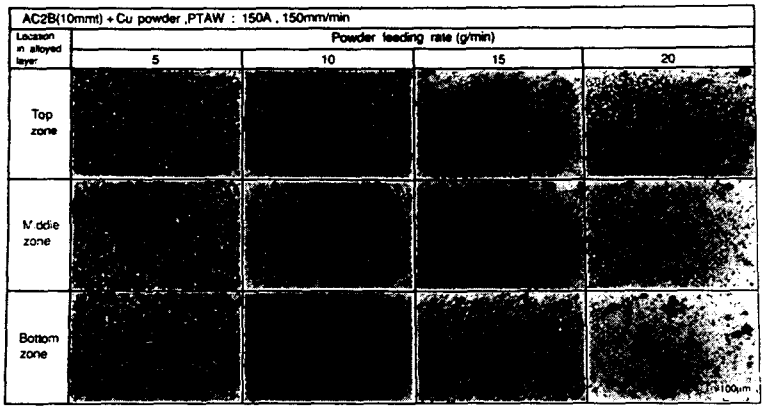

Fig. 9 Microstructures of Cu alloyed bead at different powder feeding rate.

Al_8 and partly Cr deposited on its top surface.

As a result of the comparison with phase diagram and the structure of alloyed bead, the primary phases coincided with predicted phases from phase diagram, but some phases which should disappear due to peritectic reaction with their Cr contents still remained. This means that peritectic reaction was not accomplished perfectly by rapid cooling rate in PTA process.

3.3.2 Cu alloyed bead

Figure 9 shows the microstructures at each zone with different feeding rate. Hyper-eutectic structure showing densely dispersed θ phase ($CuAl_2$) appeared at more than 10 g/min. In Cu alloyed bead, uniform microstructure was obtained in whole crosssection of alloyed bead with all the overlaying conditions used. This also shows the good agreement with a uniform distribution of Cu in alloyed bead as shown in **Fig. 10** with EPMA. Moreover, no cracking was observed in Cu alloyed bead within the overlaying conditions used in this study.

Figure 11 shows the Al-Cu phase diagram (a) and SEM microstructure with 38.2wt%Cu content (b) at 10 g/min, in which primary θ phase surrounding by $\alpha(Al)+\theta$ eutectic was observed.

3.3.3. Ni alloyed bead

Figure 12 shows the microstructures at each zone of Ni alloyed bead with different feeding rate. Needle structure

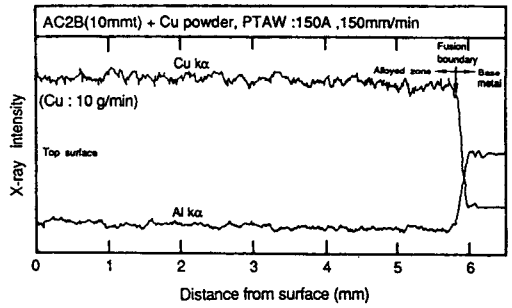

Fig. 10 Distributions of Cu and Al in Cu alloyed bead at powder feeding rate, 10 g/min.

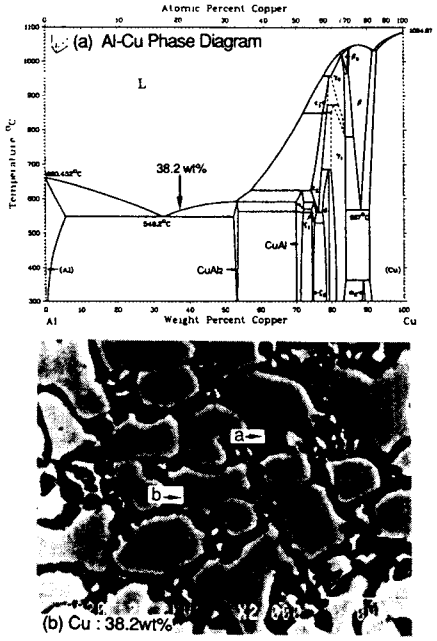

Fig. 11 SEM microstruuctures and mean Cu content of Cu alloyed bead showing relationship between phase diagram (a) and phase formed (b), a: $\alpha(Al)+CuAl_2$, b: $CuAl_2$.

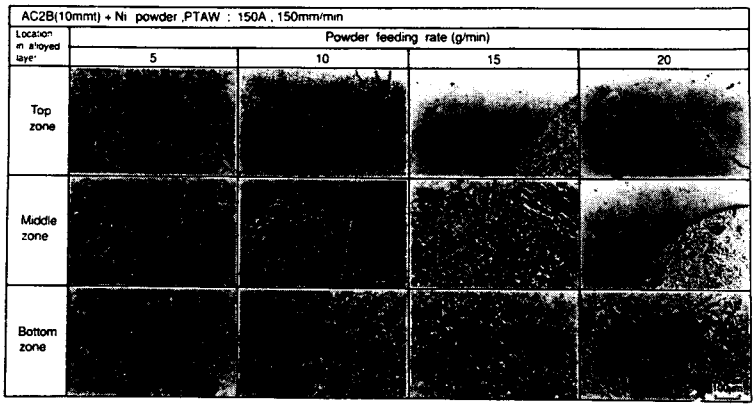

Fig. 12 Microstructures of Ni alloyed bead at different powder feeding rate

was dominant at 5 g/min, but at more than 10 g/min globular or layer compounds appeared in the top and middle zones and became dominant as the increasing feeding rate. In these structures cracking was also observed.

Figure 13 shows the distributions of Ni and Al in alloyed bead with 10 g/min. Ni content was decreased from the surface toward the bottom zone as same as the Cr distribution in Fig. 10.

Figure 14 shows the Al-Ni phase diagram (a) and SEM microstructures with mean Ni contents of 20.7wt% (b), 45wt% (c) and 64.6wt% (d) corresponding to the bottom, middle and top zones. At 20.7wt% Ni, the structure consisted of primary $NiAl_3$ surrounding by $\alpha(Al)+NiAl_3$ eutectic. At increased Ni content of 45wt%, primary phase was Ni_2Al_3 instead of $NiAl_3$, and Ni_2Al_3 was surrounded by $NiAl_3$ formed by peritectic reaction. In composition range of this peritectic reaction, even at less than 42wt% the same structure was formed because of unaccomplised peritectic reaction as observed in Al-Cr system. Partly, the island of $\alpha(Al)+NiAl_3$ eutectic was formed because of irregular segrigation in alloyed bead.

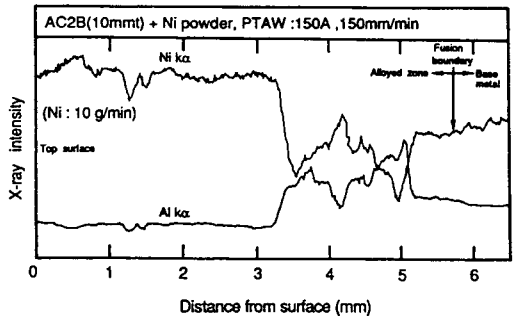

Fig. 13 Distributions of Ni and Al in Ni alloyed bead at powder feeding rate, 10 g/min.

At much higher Ni content as 64.6wt% in the top zone, single compound layer of NiAl was formed.

These structures in Ni alloyed bead showed good agreement with those predicted ones from phase diagram excluding the structure due to unaccomplised peritectic reaction as same as in Al-Cr system.

3.4 Hardness of alloyed bead

Figure 15 shows hardness distributions of Cr, Cu and Ni alloyed beads at different powder feeding rate.

In the case of Cr alloyed bead, hardness was increased with increasing feeding rate. At 5 g/min maximum hardness was about Hv280 and hardness distribution was comparably smooth due to the uniform needle structure. At 10 g/min, maximum hardness reached Hv510 in upper zone where dense needle structure was formed. At more than 15 g/min, high hardness as Hv700–740 in maximum but much rough hardness distribution were observed. This depended on the irregular structure of globular and layer

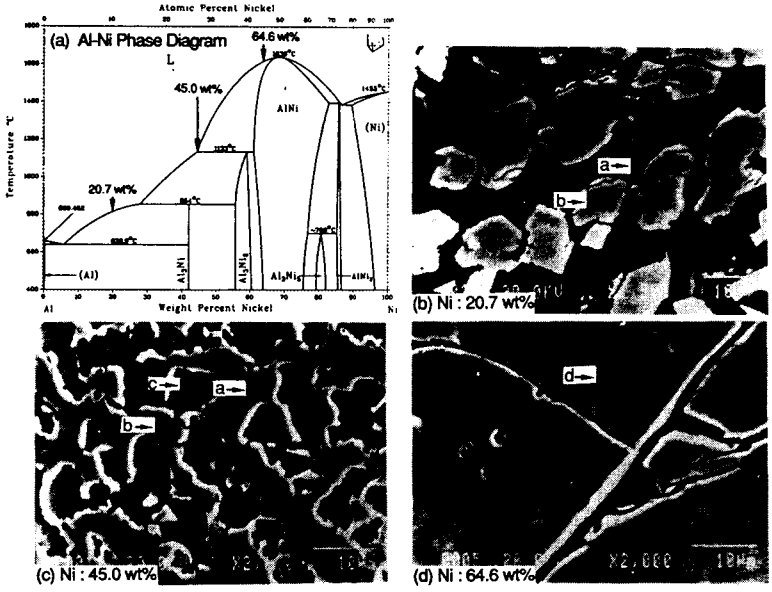

Fig. 14 SEM microstructures and mean Ni content at bottom (b), middle (c) and top zones (d) of Ni alloyed bead showing relationship between phase diagram and phase formed, a: $\alpha(Al)+NiAl_3$, b: $NiAl_3$, c: Ni_2Al_3, d: NiAl.

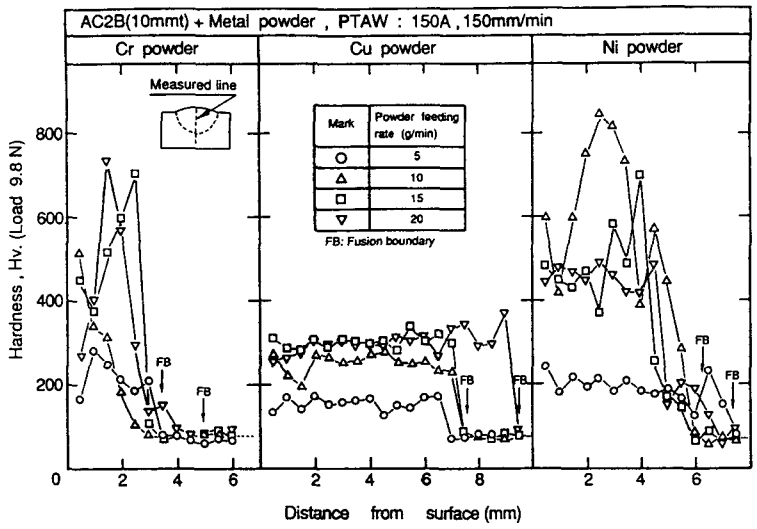

Fig. 15 Hardness distributions on crosssection of Cr, Cu and Ni alloyed beads at different powder feeding rate.

compounds. The hardness in surface zone was inclined to be lower than that in inner zone. This tendency was also observed in Ni alloyed bead. It is considered due to the macrosegrigation caused by the specific weight between alloying powder (Cr: 7.19, Ni: 8.9) and Al (2.7).

In the case of Cu alloyed bead, smooth hardness distribution through bead in each feeding rate was obtained. At 5 g/min, hypo-eutectic structure with Hv120–180 was formed and at more than 10 g/min the structure was changed to hyper-eutectic where primary θ phase (Hv400–600[21]) was densely solidified. However, their hardness were saturated to Hv250–350. These smooth hardness distribution corresponded to uniform Cu distribution in alloyed bead.

In the case of Ni alloyed bead, uniform hardness distribution of about Hv200 was obtained at 5 g/min, in which condition needle-like primary $NiAl_3$ (Hv700–770[21]) was distributed uniformly in alloyed bead. At more than 10 g/min, however, globular and layer structures of Ni_2Al_3 (Hv1100[21]) and NiAl (Hv300–700[31]) began to formed instead of needle structure. Therefore, hardness was much increased but became very rough in the range of Hv400 to 850 corresponding to the irregular distribution of hard globular and layer compounds.

Therefore, it is made clear that Cu is much more easily and uniformly alloyed in molten Al pool than Ni and Cr in spite of the largest specific weight (8.96). This reason is due to the existence of low temperature eutectic reaction as mentioned in 3.2.

Relation between hardness, alloying content and the dominant structure in alloyed bead was shown in **Fig. 16** (a), (b) and (c) for Cr, Cu and Ni alloyed beads, respectively, in which dark marks indicate the occurrance of cracking.

In the case of Cr in (a), hardness was increased monotonously up to 60wt%Cr. Cracking free range was less than about 20–25wt%Cr, in which structure was needle one of primary $CrAl_7$ dispersed in Al matrix and hardness of cracking free bead was limited to Hv250–300 in maximum. In 30–60wt%Cr, the structure consisted of dense needle structure and hardness was increased to Hv300–400, though cracking was occurred. In more than 60wt%Cr, hardness was abruptly increased to Hv500–830 because of the formation of globular Cr_5Al_8 phase, in which cracking also occurred.

In the case of Cu in (b), hardness was increased monotonously up to Hv350 at about 40wt% in hyper-eutectic structure and there was no cracking occurred.

In the case of Ni in (c), hardness was increased monotonously up to 40wt%. Cracking free range was less than 20–25wt% within the composition range of eutectic reaction and maximum hardness was Hv250–300. In more than 40wt%Ni, hardness abruptly increased to Hv400–850 because of the formation of dense needle structure ($NiAl_3+Ni_2Al_3$) and globular or layer compounds (Ni_2Al_3+NiAl), where cracking occurred.

3.5 Wear resistance of alloyed bead

Figure 17 shows the relation between the specific wear and the hardness of Cr, Cu and Ni alloyed bead under the kept wear conditions of wear load 9.8N, sliding distance

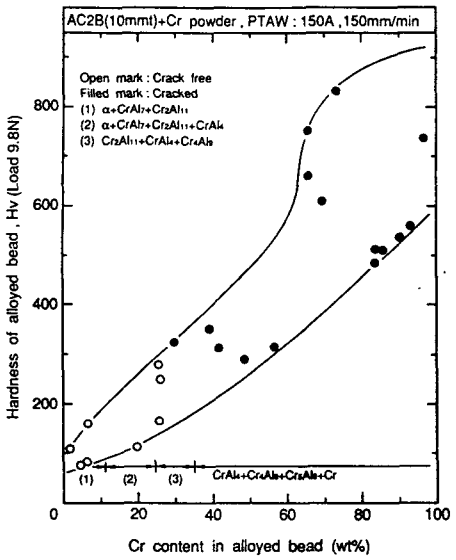

(a) Cr alloyed bead

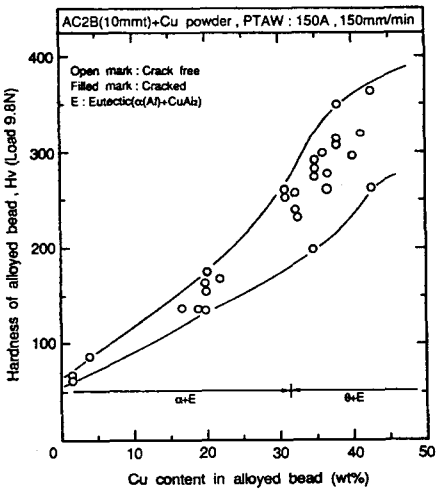

(b) Cu alloyed bead

Fig. 16 Relation between hardness and alloying content of alloyed bead.

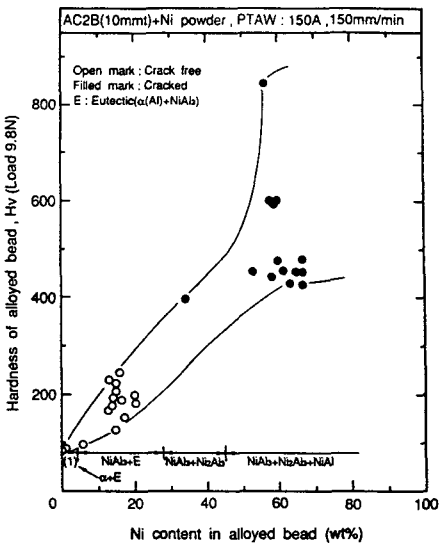

(c) Ni alloyed bead

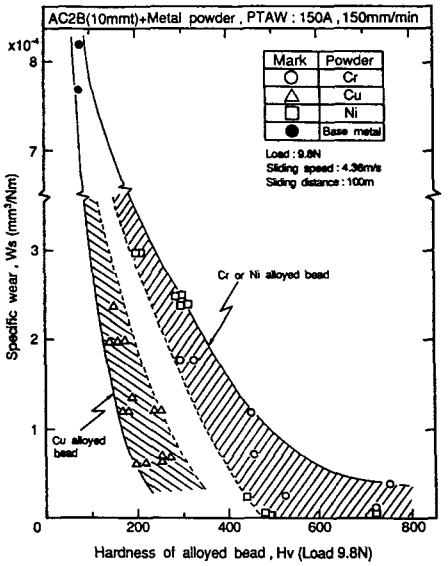

Fig. 17 Relation between specific wear of Cr, Cu and Ni al loyed beads and their hardnesses.

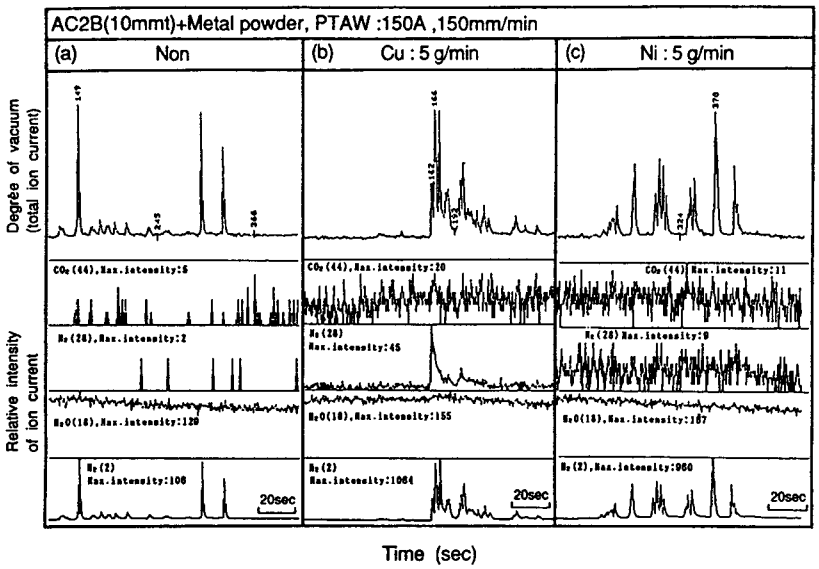

Fig. 18 Changes of total ion current corresponding to degree of vacuum and ion currents of each mass number corresponding to CO_2(44), N_2(28), H_2O(18) and H_2(2) against time during drilling of (a) unalloyed, (b) Cu and (c) Ni alloyed bead in vacuum chamber measured with mass spectroscopy.

100 m and sliding speed 4.36 m/sec. In this high sliding speed, adhesion wear property can be evaluated.

Specific wear was decreased as increasing hardness in all alloyed beads measured. Especially remarkable decrease in specific wear was obtained in Cu alloyed bead and was about 1/10 to that of base metal when hardness of alloyed bead was about Hv300. On the contrary, specific wear of Cr and Ni alloyed beads was larger than that of Cu alloyed bead even at the same hardness. It is considered that the reason of excellent wear resistance of Cu alloyed bead was due mainly to the fine hyper-eutectic structure in which hard fine θ phase were densely dispersed in fine α(Al)+θ eutectic structure as a matrix and in addition to this the strengthening effect of α(Al) by Cu solution also affected. As Ni and Cr have almost no effect to strengthening the matrix which surround the needle compounds, comparably low specific wear was obtained in harder alloyed bead consisted of globular and layer compounds structure. The existence of blow hole may increase the specific wear by gnawing away by the counter disc.

3.6 Porosity in alloyed bead

Number of large blow holes were observed in Cr and Ni alloyed beads, however, in Cu alloyed bead, both the size and the number of blow holes were decreased as shown in Fig. 5. These differences were considered due to the morphology of alloying powder as shown in Fig. 1.

In order to make clear the cause of blow hole, the residual gas analysis in blow holes was carried out. **Figure 18 (a), (b) and (c)** show the typical evaluated results by mass spectoroscopic analyzer for unalloyed remelted bead, Cu and Ni alloyed beads with 5 g/min, respectively. Identified residual gas species were CO_2(mass number 44), N_2(28), H_2O(18) and H_2(2). Other gas species were not detected within the background level. An upper figure in Fig. 18 indicates the change in relative degree of vacuum represented by total ion current vs. time during drilling of alloyed bead, and lower four figures show the change in relative intensity of ion current for each mass number corresponding to CO_2, N_2, H_2O and H_2 vs. time simultaniously, in which maximum intensity indicates the highest peak value in each figure.

Figure 18 (a) shows the results of blow holes formed in unalloyed bead. Abrupt decreases in degree of vacuum corresponded only to the exhaustion of H_2, and CO_2 and N_2 were ignored because of their extremely low intensity. This result indicates that residual gas in blow hole formed in remelted bead is H_2, which probably caused by the preformed blow holes in cast base metal.

Nextly, in the case of powder alloyed bead, two types were observed i.e. one was only the exhaustion of H_2 as shown in (c) for example and the other was the exhaustion of H_2 accompanied by N_2, of which intensity was much low as shown in (b). In each case, the intesity of H_2 is 9 to

10 times as high as in (a) without powder. This high intensity of H_2 corresponds to much porosity in alloyed bead, and the source of N_2 is considered to due to the air gas absorbed into shielding gas, though its cause was not made clear in this study.

The major cause of blow hole formed in weld bead of Al alloy arc welds is considered to be H_2[15], and absorbed H_2O and organic materials on the surface of base and filler materials is considered to the cause of H_2[15]. In this study, absorbed H_2O in powder surface was considered to be the dominant cause of blow hole. This was supported by the evidence that Cu powder with spherical shape made less porosity than Ni and Cr powders with irregular shapes possessing many sites for H_2O absorption as shown in Fig. 1.

Therefore, to prevent the porosity in alloyed bead the usage of spherical shape powder and vacuum dry treatment of powder just before the use will be expected, and these effects should be treated in latter paper.

4. Conclusions

The formation of a thicker hard alloyed layer have been investigated on the surface of Al cast alloy (AC2B) by PTA overlaying process with Cr, Cu and Ni metal powders under the conditions of overlaying current 125–200A, overlaying speed 150 mm/min and powder feeding rate 5–20 g/ min. Hardening characteristics, wear resistance and defects such as cracking and porosity of alloyed bead have been examined in relation to the microstructures of alloyed bead.

Main results obtained were summarized as follows:

1) There was an optimum overlaying condition to get a good alloyed bead with smooth surface, which became easy to be formed at an increasing overlaying current and a decreasing powder feeding rate under a constant overlaying speed.
2) Cu powder was the most superior one in metal powders used due to the wide optimum overlaying condition range, uniform hardness distribution of Hv250–350, good wear resistance and freedom from cracking in alloyed bead, of which microstructure consisted of fine hyper-eutectics.
3) Irregular hardness distribution was usually obtained in Cr or Ni alloyed beads, of which hardness was increased as Cr or Ni contents and reached to maximum hardness of about Hv400–850 at about 60wt%Cr or 40wt%Ni in alloyed bead.
4) Cracking occurred in Cr or Ni alloyed beads with higher hardness than Hv250–300 at more than 20–25wt%Cr or Ni contents in alloyed beads, of which structure consisted of globular and/or layer intermetallic compounds. Cracking free alloyed bead was obtained in the structure where primary intermetallic compounds were dispersed in the Al matrix.
5) Wear resistance of alloyed bead was remarkably increased as the increasing hardness and reached ten, five and three times as same as that of base metal in Cu, Cr and Ni alloyed beads, respectively.
6) The structure of Cu alloyed bead coincided to Al-Cu phase diagram. In the case of Cr or Ni alloyed beads, primary phases coincided to Al-Cr and -Ni phase diagrams, but following peritectic reaction was unaccomplished because of rapid solidification rate.
7) Alloying powder with rough surface made much porosity, but powder with spherical shape and smooth surface made less porosity. The residual gas in blow hole was mainly hydrogen and sometines accompanied by nitrogen in lower level.

Acknowledgements

The authors would like to express their thanks to Mr. Kenji Tohmoto, Technical assistant and Mr. Kazuya Konishi, Strudent of Kinki University for their helpful assistants for the experiment, and also ISUZU Central Research Institute Co. Ltd. for offering base Al alloy and Nippon Steel Welding Products & Engineering Co. Ltd. for offering PTA overlaying apparatus and gas analysis of blow hole.

The financial support provided for the present work through Scientific Research Fund from Japan Light Metal Association is gratefully acknowledged.

References

1) Japan Research and Development Center for Metals: Technical research report on Al surface hardening technology in mm order in thickness, (1989).
2) F. Matsuda: J. Japan Institute of Light Metals, 40 (1990), 746.
3) W. Hiller: Rev. Souldure, 36 (1980), 159.
4) B. Vinet and Paidassi: Rapidly quenched metals, Elsevier science publisher, (1985), 937.
5) M. H. Sohi and T. Bell: Proc. of 2nd International Conf. on Power Beam Technology, The Welding Institute, UK, (1990), 286.
6) J. D. Ayers: Thin Solid Films, 84 (1981), 323.

7) A. W. Walker, W. H. Steen and D. R. F. West: Aluminum Technology'86, The Institute of Metals, London, (1986), 88. 1.

8) F. Matsuda and K. Nakata: Trans. JWRI, 17 (1988), 457.

9) E. Gaffet, J.M. Pelletier and S.B. Jobez: Applied Surface Science, 43 (1989), 248.

0) M. Pierantoni and Z. Blank: Proc. of the 2nd IFHT Seminar, Lisbon, (1989), 317.

1) G. Ricciardi, M. Cantello, G. Molino, W. Varani and E. Carlet: Proc. of 2nd IFHT Seminar, Lisbon, (1989), 415.

12) S. Shimizu, K. Nagai, F. Matsuda and K. Nakata: J. of Japan Institute of Light Metals, 40 (1990), 761.

13) T.B. Massalski: Binary Alloy Phase Diagram (Vol. 1), ASM, (1986), 104, 106, 142.

14) L.M. Mondolfo: Aluminum Alloys, Structure and Properties, Butterworths, (1976), 250, 338.

15) Japan Welding Society: Handbook on Welding • Joining, Maruzen, (1990), 1010.